Non–Classical Longitudinal Magneto–Resistance in Anisotropic Black Phosphorus

F. Telesio [1,*], N. Hemsworth [2], W. Dickerson [2], M. Petrescu [3], V. Tayari [2], Oulin Yu [3], D. Graf [4], M. Serrano–Ruiz [5], M. Caporali [5], M. Peruzzini [5], M. Carrega [1], T. Szkopek [2], S. Heun [1], G. Gervais [3],

[1] NEST, Istituto Nanoscienze–CNR and Scuola Normale Superiore, I-56127 Pisa, Italy

[2] Department of Electrical and Computer Engineering, McGill University, Montréal, Québec, H3A 2A7, Canada

[3] Department of Physics, McGill University, Montréal, Québec, H3A 2T8, Canada

[4] National High Magnetic Field Laboratory, Tallahassee, FL 32310, United States

[5] Istituto di Chimica dei Composti OrganoMetallici–CNR, I-50019 Sesto Fiorentino, Italy

Key words: black phosphorus, longitudinal magneto–resistance, anisotropy

[*]Corresponding author: e–mail francesca.telesio@nano.cnr.it; gervais@physics.mcgill.ca

Resistivity measurements of a black phosphorus (bP) field–effect transistor 16 nm thick in parallel magnetic fields up to 45 T are reported as a function of the angle between the in–plane field and the source–drain (S–D) axis of the device. The crystallographic directions of the bP crystal were determined by Raman spectroscopy, with the zigzag axis

found to be within 5° of the S–D axis, and the armchair axis in the orthogonal planar direction. A transverse magneto–resistance (TMR) as well as a classically–forbidden longitudinal magneto–resistance (LMR) are observed. Both are found to be strongly anisotropic and non–monotonic with increasing in–plane field. Surprisingly, the relative magnitude (in %) of the positive LMR is larger than the TMR above $\sim$32 T. Considering the known anisotropy of bP whose zigzag and armchair effective masses differ by a factor of approximately seven, our experiment strongly suggests this LMR to be a consequence of the anisotropic Fermi surface of bP.

Introduction. Magnetoresistance (MR) is a phenomenon in which a material's resistivity increases or decreases due to the presence of a magnetic field $\mathbf{B}$. Transport measurements typically require the presence of an electric field $\mathbf{E}$ so as to establish an average current with charge velocity v along a preferred direction. The overall force on the charge carriers q (electrons or holes) is simply given by the Lorentz force, $\mathbf{F} = q(\mathbf{E} + \mathbf{v} \times \mathbf{B})$. From this stems two important limiting cases: one where the current flow is perpendicular to $\mathbf{B}$ and for which the magnitude contribution of the Lorentz force is maximal, and the other where it is parallel to $\mathbf{B}$, and there is no magnetic contribution to the Lorentz force. This simple classical picture therefore implies that MR is forbidden in the latter case. However, decades of research have shown that a material can develop a longitudinal magnetoresistance (LMR) when the current and the magnetic field are parallel. The exact set of conditions for which a non–classical LMR can or cannot be observed remains a highly debated topic which has gained renewed interest recently within the context of Weyl semimetals and topological insulators [1–3].

Pal and Maslov [4] have studied theoretically the non–classical LMR on generic grounds. They proposed a set of necessary and sufficient conditions within the context of Fermi surface (FS) morphology for a three–dimensional system. While not all anisotropy leads to a LMR, it was shown that an angular anisotropy of the FS along the magnetic field direction is a sufficient condition. Black phosphorus (bP) provides a key system for this since its Fermi surface (FS) is highly anisotropic with effective masses for holes $m_{ac} = 0.11 m_0$ and $m_{zz} = 0.71 m_0$ (m_0 is the bare electron mass) along the armchair (ac) and zigzag (zz) directions, respectively [5]. LMR has been observed previously in bulk crystals of bP [6, 7] yielding only limited progress in its understanding. This is the subject of this work, where an experiment was designed to perform magneto–transport measurements in a 16–nm–thick bP device in the presence of a purely parallel magnetic field that could be rotated in the plane of the bP flake, and up to 45 T field. A strong classically–forbidden LMR was found whose non–monotonic field dependence closely matches a parabolic behavior. Even though LMR has been studied for decades in three–dimensional systems, to our knowledge there is no rigorous theory in two–dimensional anisotropic systems and as such our results are calling for future theoretical work in this direction.

Device structure. The geometry of the field–effect transistor (FET) device is shown in Figure 1(a). Details on device fabrication are provided in the supplementary information (SI). The flake thickness was carefully determined from the atomic force microscopy (AFM) measurements shown in the SI, and is $t = (16 \pm 1)$ nm in the channel region, i.e. around 30 layers, given that the layer–to–layer spacing in bP is 0.524 nm [8]. The channel length and average weighted width are $L = 25.4$ μm and $W = 4.4$ μm, respectively. The transistor includes a conventional back gate and two additional top gates, labeled TG1 and TG2 in Figure 1(a), employing a combination of PO

$_x$ and Al_2O_3 as oxide dielectrics [9]. For the measurements presented here, TG1 is not used. We define φ as the angle between the source–drain (S–D) axis of the device and the in–plane magnetic field used in the experiment (see Figure 1(a) and Figure 2(a)). With this convention, at $\varphi = 0^\circ$ the magnetic field is parallel to the S–D axis and hence to the current ($\mathbf{B} \parallel \mathbf{I}$), whereas at $\varphi = \pm 90^\circ$ the magnetic field is perpendicular to the S–D axis and the current ($\mathbf{B} \perp \mathbf{I}$). For clarity, the same convention has been used in displaying the polarized Raman measurements shown in Figure 1(c) and (d).

Raman characterization. The crystal orientation with respect to the source–drain axis was determined via polarized Raman spectroscopy. Here, the crystallographic orientation of the bP crystal, shown in Figure 1(b), was determined by measuring the Raman peak intensities associated with the in–plane vibrational modes of black phosphorus (A_g^2 and B_{2g}) [10] with respect to the linear polarization of the incident laser [11, 12]. In particular, the maximum of the A_g^2 mode corresponds to the armchair direction [10, 13, 14]. These Raman data are shown in Figure 1(d) as a function of polarization angle φ, whereby for 0° the polarization of the incoming laser beam is parallel to the axis of the bP FET channel (dashed line in Figure 1(a)). From these data, we determine the bP crystal orientation to be such that the zigzag direction is at angle $\theta = (-5 \pm 3)^\circ$ from the S–D channel axis, as can be seen in Figure 1(d) (see also SI, Fig. S3).

Magneto–transport measurements. During low–temperature magneto–transport measurements, the gate voltage dependence revealed an inherent p-type character for the bP FET. The device exhibited an intrinsic carrier concentration $n = 2.2 \times 10^{12}$ cm^{-2} and a field–effect mobility

$\mu = 83$ cm^2/(Vs) at $T = 1.64$ K and $B = 11.4$ T, as provided in the SI. In all displayed measurements, except when explicitly stated, TG1 and the back gate were kept to ground, whereas TG2 was set to -1 V to increase the bP conductance. The device was mounted on a calibrated step–by–step rotator (shown in Figure 2(b)) that could rotate the sample with the magnetic field axis in the plane of the device. The rotator had an angular resolution within 0.02° which is much less than the systematic errors on φ arising from the crystallographic orientation measurements of bP by Raman spectroscopy. The experiment was performed at low temperatures down to 300 mK and up to a 45 T magnetic field in the hybrid magnet of the National High Magnetic Field Laboratory in Tallahassee, shown in Figure 2(c). The in–plane magneto–transport was investigated by performing several angular sweeps at various magnetic fields, as well as magnetic field sweeps at various angles, to check for data consistency. The normalized magneto–resistance of the device, defined as $\Delta R / R = (R(B) - R(0)) / R(0)$, with $R(0) \equiv R(B = 0) = 173.3$ kΩ, is shown for various magnetic fields in Figure 3 on the left axis of the graph, whereas the right axis displays the resistance values. Overall, the MR is observed to have a strong dependence on the angle φ and varies non–monotonically with the increasing in–plane magnetic field. Given that a misalignment of 1° at 45 T would result in a perpendicular field component of 0.78 T, the possible presence of this out–of–plane field was considered. Although the presence of such an out–of–plane component is possible, it cannot itself give rise to the phenomena investigated here. In particular, a potential correction due to weak localization at high magnetic field is expected to decrease the resistance, and therefore it cannot explain the positive longitudinal magneto–resistance observed at high field.

Upon closer inspection of Figure 3 it becomes apparent that the maxima and minima in MR are not exactly aligned at $\varphi = 0^\circ$ and 90° (as indicated by the dotted vertical lines in the figure) but instead are slightly shifted to a lower value (as indicated by the arrows). Tracking the angular position of the maximum in MR close to -90° and the minimum close to 0°, their angular positions are found to be nearly constant at all magnetic fields, and given by $(-94.4 \pm 2.0)^\circ$ and $(-2.8 \pm 2.0)^\circ$, respectively. The $\pm 2^\circ$ quoted here was estimated from the possible orientation error in mounting the device on the high magnetic field sample holder. This significant deviation from the precise values of the device axis suggests that neither the device axis nor the current direction define the relevant coordinate system for the MR. In fact, these angles correspond within error to the orientation of the bP crystal and the directions of zigzag and armchair axes of the bP crystal, indicating that these are the physically–relevant directions determining the magneto–resistance.

Figure 4 displays cross–sections of Figure 3 for the parallel ($\varphi = 0^\circ$) and perpendicular ($\varphi = -90^\circ$) configurations of the magnetic field with respect to the current direction. The longitudinal magneto–resistance ($\mathbf{B} \| \mathbf{I}$) is first negative, passes through a minimum at approximately 11 T, and then increases to reach a positive value at approximately 26 T. The LMR is found to take larger value than the transverse magneto–resistance ($\mathbf{B} \perp \mathbf{I}$) at a crossover field of approximately 32.5 T. Remarkably, the magnetic field dependence of the LMR can be well described by a shifted parabola centered at $B = (11.9 \pm 0.3)$ T (red line). In contrast, the TMR is nearly constant up to 11 T field (where the LMR reached its minimum value), and then increases roughly linearly with the in–plane magnetic field increasing.

Resistance measurements taken at fixed angle as a function of magnetic field confirm this trend. These measurements are shown in Figure S4(d) of the SI. At angles φ close to 0° and -90°, the data display a similar crossover, whereas at $\varphi \approx -180^{\circ}$ and 0° the data highlight the 180° periodicity of the phenomenon. Finally, upon reversal of the magnetic field, the magneto–resistance showed no significant dependence on the field direction, see SI Figure S4(e), except for a slight overall shift that is attributed to a small change in carrier density occurring during a temperature cycling of the device from base to ~ 40 K temperatures. Since the transport measurements were performed in a two–point configuration, the robustness of the observed LMR and TMR against magnetic field polarity ensures that solely the in–plane resistivity played a role in the experiment.

Transport regime and length scales. To establish the regime of charge transport in the bP flake, we compare the relevant length scales obtained from the experimentally determined carrier density n and mobility μ. We apply a two–dimensional Drude model justified here by a self–consistent Schrödinger–Poisson calculation showing that the charge density in bP flakes on SiO_2 is concentrated within a surface accumulation layer with mean thickness $\langle z \rangle \simeq 3$ nm [15]. Within the effective mass approximation, the hole dispersion is given by $E = \delta + \hbar^2 k_{zz}^2 / 2m_{zz} + \hbar^2 k_{ac}^2 / 2m_{ac}$ [16], with δ the band gap, quantifying the anisotropy in charge carrier motion along zigzag and armchair directions.

The Fermi wavevector is itself anisotropic, with the relevant Fermi wavevector being $k_{F,zz}$ for charge carriers moving in the zigzag direction with current flow in the bP flake. The

wavevector is $k_{F,zz} = (m_{zz} / m_{ac})^{1/4} (2\pi n)^{1/2} = 0.59\ \mathrm{nm}^{-1}$, which corresponds to a Fermi wavelength $\lambda_{F,zz} = 2\pi / k_{F,zz} = 10.6\ \mathrm{nm}$. The Fermi wavelength is larger than the mean thickness $\langle z \rangle$ of the accumulation layer, and smaller than the flake thickness t. The Fermi velocity $v_{F,zz}$ along the zigzag axis is $v_{F,zz} = \hbar k_{F,zz} / m_{zz} = 9.7 \times 10^4\ \mathrm{ms}^{-1}$. The elastic scattering time $\tau_{zz} = m_{zz} \mu / e = 3.3 \times 10^{-14}\ \mathrm{s}$ and the elastic mean free path $\ell_{e,zz} = v_{F,zz} \tau_{zz} = 3.2$ nm [17], where the mobility $\mu = \mu_{zz}$ was measured for current flow along the zigzag axis. The mean free path $\ell_{e,zz}$ is similar to the thickness of the accumulation layer $\langle z \rangle$.

The Ioffe–Regel criterion for localization [18, 19] can be used to ascertain the regime of charge transport. We find $k_{F,zz} \ell_{e,zz} = 1.9$, indicating that transport within our bP device is diffusive, albeit close to the crossover from diffusive to localized transport ($k_F \ell_e = 1$). We can compare the length scales of charge carrier transport with the magnetic length $\ell_B = \sqrt{\hbar / eB}$, which decreases from 11.4 nm at $B =$ 5 T to 3.8 nm at $B =$ 45 T. Only at the highest fields used in our experiments does the magnetic length approach the thickness of the accumulation layer.

Spin–orbit scattering. A negative magneto–resistance in the strongly localized regime has been observed before, and has been ascribed to the orbital MR due to quantum–interference among random paths in the hopping process [20, 21]. In particular, it was reported that an anisotropy in the MR is indicative of this magneto–orbital mechanism and that this orbital MR is always negative [21]. Later work suggested that inclusion of spin–orbit scattering in the theory would lead to a positive MR [22, 23]. Such positive MR in the strongly localized regime has been observed in many disordered materials [24]. However, this reasoning is unlikely to be applicable here given

that spin–orbit coupling in bP is so weak [5, 25]. Besides, the in–plane anisotropy of the g-factor of bP is also negligible ($g_{ac} \approx g_{zz}$) [26, 27] and close to the bare electron value $g = 2$, indicative of negligible exchange enhancement [26].

Anisotropic Fermi surface. Non–classical LMR has been observed in a variety of systems ranging from three–dimensional metals, topological materials, and semiconductors (see [2] for a recent discussion). Already in the 1960's this phenomenon was attracting interest in the context of metals with non–trivial Fermi surfaces [28], and subsequently in semiconductors with non–parabolic bands [29]. More recently, it has been discussed for massless Dirac and Weyl fermionic systems [1, 2, 30]. In 2010, Pal and Maslov [4] derived the necessary and sufficient conditions for the occurrence of LMR within the context of Fermi surface morphology of a three–dimensional electronic system; while they have shown that an anisotropic Fermi surface is a prerequisite, not all types of anisotropy will give rise to the effect. They specified that an angular anisotropy of the Fermi surface along the magnetic field direction is a sufficient condition in three dimensions. Our case, for which the electronic system is defined by a two–dimensional hole gas confined at the bP/SiO_2 interface, provides an interesting example of anisotropic FS since the bP Fermi surface is elliptical and its effective masses in the armchair and zigzag directions differ by a factor of approximately seven.

While Pal and Maslov studied the conditions for LMR to occur on generic grounds for a three–dimensional system, a quantitative theoretical description for LMR in two–dimensional systems with anisotropic FS is still lacking. Moreover, Goswami et al. [2] state that for a 3D metal the existence of a finite LMR is purely a quantum–mechanical effect and a direct consequence of

the axial anomaly. Furthermore, they showed that in the presence of both neutral and ionic impurities, the LMR becomes first negative for low fields, and then positive for high fields after passing through a minimum, which is reminiscent of what is observed in the LMR data shown in Figure 4. We caution, however, that their theory was developed for the quantum limit where $\omega_c\tau \gg 1$, with ω_c the cyclotron frequency and τ the elastic scattering time. Nevertheless, the authors of [2] underline the good agreement of their results with calculations of Spivak and co–workers in the semi–classical [1] and diffusive regime [3], both valid for $\omega_c\tau \ll 1$. These recent theoretical advances suggest that a similar framework should be developed in 2D systems, especially given the present interest in 2D atomic crystals of all kinds. For instance, it is known that applying a purely parallel magnetic field on a two–dimensional electron gas (2DEG) can lead to a magneto–orbital coupling sufficient to generate a substantial magneto–resistance, as proposed theoretically by Das Sarma and Hwang [31] and found experimentally in GaAs 2DEGs with finite widths [32]. Black phosphorus being a simple system to test the effects of FS anisotropy, it is in our view likely that FS anisotropy could lead to the MR modulation found in this work, even though no quantitative theory in 2D exists at the moment.

Conclusions. The classically–forbidden LMR has been studied in different material systems for decades, and only recently the conditions under which it can be observed were explored theoretically in three dimensions. One clear route towards an LMR in 3D involves an anisotropic Fermi surface, and in its simplest expression an anisotropic FS in 2D can be thought out of an ellipse. Our work on black phosphorus at high–magnetic field provides an important example for the appearance of LMR in a two–dimensional anisotropic system, and such observation of a longitudinal magneto–resistance for all fields inspected is confirmed. This LMR was discovered to

be strongly anisotropic, non–monotonic, positive beyond ~ 26 T and dominant in strength beyond ~ 30 T field. Even though the magnetic length at the highest magnetic field used here (45 T) is more than one order of magnitude larger than the phosphorus bond length, this LMR work demonstrates once more the potential generated by high magnetic fields in the understanding of band structure effects on charge transport in atomic crystals. Our experimental data strongly suggests that anisotropy most likely plays an important role in the appearance of LMR, thereby calling for theoretical descriptions of magneto–transport properties in the presence of anisotropic Fermi surfaces to be developed.

Acknowledgements We are grateful to Danil Bukhvalov, Alina Mre n′ ca–Kolasi n′ ska, and Bart łomiej Szafran for helpful discussions. This work was funded by NSERC (Canada), CIFAR, FRQNT (Québec), and the CRC program (Thomas Szkopek and Guillaume Gervais). A portion of this work was performed at the National High Magnetic Field Laboratory which is supported by NSF Cooperative Agreement No. DMR-1157490, and the State of Florida. Francesca Telesio, Manuel Serrano–Ruiz, Maria Caporali, Maurizio Perruzini, and Stefan Heun thank the European Research Council for funding the project PHOSFUN *Phosphorene functionalization: a new platform for advanced multifunctional materials* (Grant Agreement No. 670173) through an ERC Advanced Grant to Maurizio Peruzzini. Francesca Telesio acknowledges financial support by CNR–Nano through the SEED project SURPHOS. Stefan Heun acknowledges support from Scuola Normale Superiore, Project No. SNS16 B HEUN-004155. Matteo Carrega acknowledges support from the bilateral project CNR/Royal Society number IES/R3/170252.

References

[1] D. T. Son and B. Z. Spivak, Phys. Rev. B **88**, 104412 (2013).

[2] P. Goswami, J. H. Pixley, and S. Das Sarma, Phys. Rev. B **92**, 075205 (2015).

[3] A. Andreev and B. Z. Spivak, Phys. Rev. Lett. **120**, 026601 (2018).

[4] H. K. Pal and D. L. Maslov, Phys. Rev. B **81**, 214438 (2010).

[5] J. Qiao, X. Kong, Z. X. Hu, F. Yang, and W. Ji, Nat. Commun. **5**, 4475 (2014).

[6] T. Strutz, N. Miura, and Y. Akahama, Physica B **194-196**, 1185–1186 (1994).

[7] Z. Hou, B. Yang, Y. Wang, B. Ding, X. Zhang, Y. Yao, E. Liu, X. Xi, G. Wu, Z. Zeng, Z. Liu, and W. Wang, Sci. Rep. **6**, 23807 (2016).

[8] A. Morita, Applied Physics A Solids and Surfaces **39**(4), 227–242 (1986).

[9] W. Dickerson, V. Tayari, I. Fakih, A. Korinek, M. Caporali, M. Serrano-Ruiz, M. Peruzzini, S. Heun, G. A. Botton, and T. Szkopek, Appl. Phys. Lett.

112, 173101 (2018).

[10] S. Sugai and I. Shirotani, Solid State Commun. **53**, 753–755 (1985).

[11] X. Chen, X. Lu, B. Deng, O. Sinai, Y. Shao, C. Li, S. Yuan, V. Tran, K. Watanabe, T. Taniguchi, D. Naveh, L. Yang, and F. Xia, Nat. Commun. **8**, 1672 (2017).

[12] X. Wang, A. M. Jones, K. L. Seyler, V. Tran, Y. Jia, H. Zhao, H. Wang, L. Yang, X. Xu, and F. Xia, Nat. Nanotechnol. **10**, 517–521 (2015).

[13] J. Kim, J. U. Lee, J. Lee, H. J. Park, Z. Lee, C. Lee, and H. Cheong, Nanoscale **7**, 18708–18715 (2015).

[14] A. L. Phaneuf-L'Heureux, A. Favron, J. F. Germain, P. Lavoie, P. Desjardins, R. Leonelli, R. Martel, and S. Francoeur, Nano Lett. **16**, 7761–7767 (2016).

[15] V. Tayari, N. Hemsworth, I. Fakih, A. Favron, E. Gaufrès, G. Gervais, R. Martel, and T. Szkopek, Nat. Commun. **6**, 7702 (2015).

[16] A. Chaves, W. Ji, J. Maassen, T. Dumitrica, and T. Low, Theoretical overview of black phosphorus, in: 2D Materials. Properties and Devices, (Cambridge University Press, 2017), pp. 381–412.

[17] T. Ando, A. B. Fowler, and F. Stern, Rev. Mod. Phys. **54**, 437–672 (1982).

[18] M. Gurvitch, Phys. Rev. B **24**, 7404–7407 (1981).

[19] P. A. Lee and T. V. Ramakrishnan, Rev. Mod. Phys. **57**, 287–337 (1985).

[20] U. Sivan, O. Entin-Wohlman, and Y. Imry, Phys. Rev. Lett. **60**, 1566–1569 (1988).

[21] O. Faran and Z. Ovadyahu, Phys. Rev. B **38**, 5457–5465 (1988).

[22] J. L. Pichard, M. Sanquer, K. Slevin, and P. Debray, Phys. Rev. Lett. **65**, 1812–1815 (1990).

[23] P. Hernandez and M. Sanquer, Phys. Rev. Lett. **68**, 1402–1405 (1992).

[24] W. Jiang, J. L. Peng, J. J. Hamilton, and R. L. Greene, Phys. Rev. B **49**, 690–693 (1994).

[25] Z. S. Popović, J. M. Kurdestany, and S. Satpathy, Phys. Rev. B **92**, 035135 (2015).

[26] L. Li, F. Yang, G. J. Ye, Z. Zhang, Z. Zhu, W. Lou, X. Zhou, L. Li, K. Watanabe, T. Taniguchi, K. Chang, Y. Wang, X. H. Chen, and Y. Zhang, Nat. Nanotechnol. **11**, 593–597 (2016).

[27] X. Zhou, W. K. Lou, D. Zhang, F. Cheng, G. Zhou, and K. Chang, Phys. Rev. B **95**, 045408 (2017).

[28] A. B. Pippard, Proc. R. Soc. London, Ser. A **282**, 464–484 (1964).

[29] U. P. Phadke and S. Sharma, J. Phys. Chem. Solids **36**, 1–6 (1975).

[30] A. Sekine, D. Culcer, and A. H. MacDonald, Phys. Rev. B **96**, 235134 (2017).

[31] S. Das Sarma and E. H. Hwang, Phys. Rev. Lett. **84**, 5596–5599 (2000).

[32] X. Zhou, B. A. Piot, M. Bonin, L. W. Engel, S. Das Sarma, G. Gervais, L. N. Pfeiffer, and K. W. West, Phys. Rev. Lett. **104**, 216801 (2010).

Graphical Table of Contents

GTOC image:

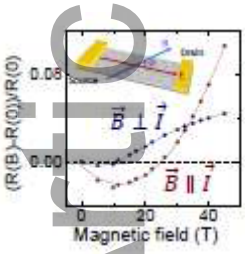

We report on magneto–transport measurements on a black phosphorus device in parallel magnetic field, up to 45 T, as a function of the angle between the source–drain axis and the magnetic field. We observe strongly anisotropic and non-monotonic transverse and (classically forbidden) longitudinal magneto–resistance with increasing in-plane field. These findings demonstrate the potential generated by high magnetic fields in the understanding of band structure effects on transport in anisotropic crystals.

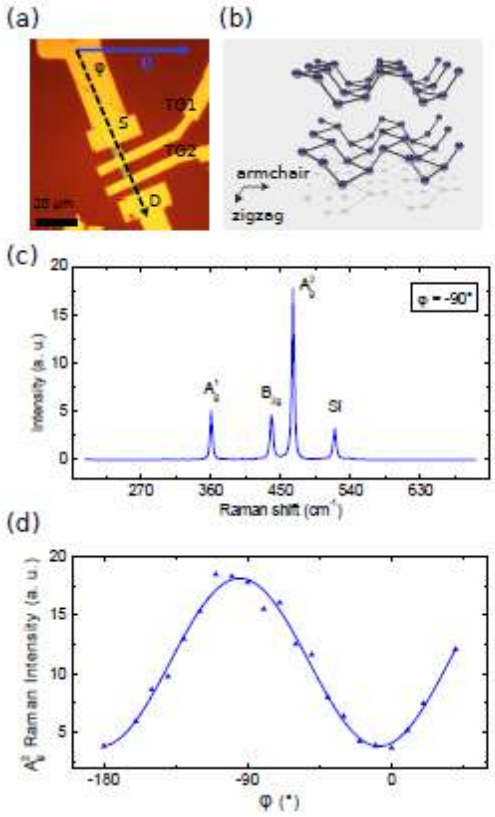

Figure 1 (**a**) Optical microscopy image of the device with labeling of source (S) and drain (D) contacts, top gates TG1 and TG2, as well as the definition of the angle φ as the angle between source–drain and the magnetic field axis. (**b**) The puckered crystal structure of black phosphorus with armchair and zigzag directions indicated. (**c**) Raman spectrum of the bP device, with baseline subtracted. The spectrum was acquired at $\varphi = -90^{\circ}$, i.e. with light polarization perpendicular to the device axis. The three bP Raman peaks are labeled, as well as the peak emanating from the Si substrate. (**d**) Polarized Raman measurement. A_g^2 intensity as a function of incoming laser light polarization angle φ. The maximum of A_g^2 is along the armchair axis, the minimum at $(-5 \pm 2)^{\circ}$ along zigzag, and therefore the S–D axis of the device is approximately aligned with the zigzag direction of the flake (see SI for additional details).

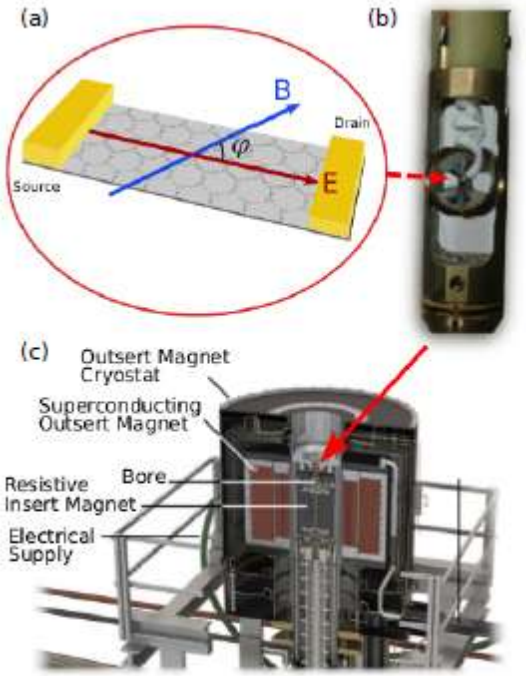

Figure 2 (**a**) Schematics of the device with electric field **E** and magnetic field **B** indicated, as well as crystallographic orientation. The angle φ is defined as the angle between source–drain and magnetic field axis. (**b**) Photo of the rotator probe as mounted in the cryostat insert. The sample is rotating with the magnetic field in the bP plane. (**c**) Schematics of the hybrid magnet of National High Magnetic Field Laboratory used for the high–field measurements. The outer, superconducting magnet provides a field in the 0 T to 11.4 T range, and together with the resistive insert a field of 45 T can be reached.

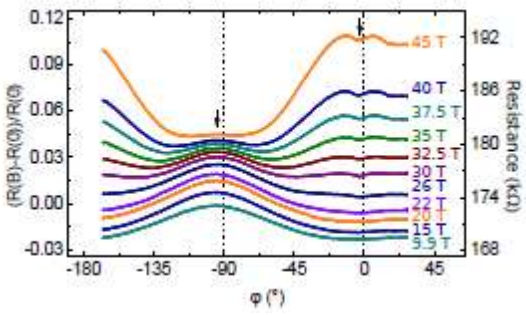

Figure 3 Magneto–resistance, defined as $(R(B)-R(0))/R(0)$, vs. the in–plane angle of rotation

φ at various magnetic fields, left axis. The resistance value is displayed on the right axis. The data was taken at 323 mK temperature.

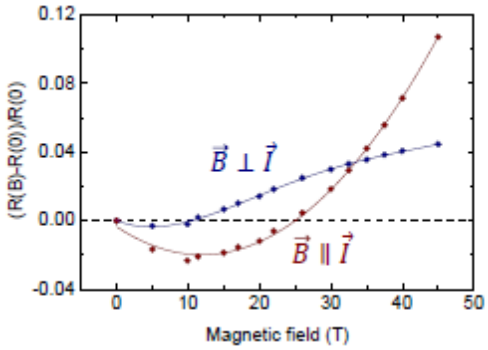

Figure 4 Magnetic–field dependence of the LMR and TMR showing distinct behaviours. It is based on the data shown in Figure 3. The red line is a fit of the LMR ($\mathbf{B} \parallel \mathbf{I}$) data with a shifted parabola centered at $B = (11.9 \pm 0.3)$ T. The blue line is a guide–to–eye for the TMR data ($\mathbf{B} \perp \mathbf{I}$).